

EXPERIMENTS ON NEOCLASSICAL ASYMMETRIC SUPERBANANA RIPPLE TRANSPORT IN ELECTRON PLASMA

A.A. Kabantsev, C.F. Driscoll

University of California at San Diego, La Jolla, CA 92093, USA
E-mail: akabantsev@ucsd.edu

Ripples in magnetic or electrostatic confinement fields give rise to trapping separatrices, and the conventional neoclassical helical ripple transport describes phenomena coming from the *collisional* trapping/detrapping of particles in the helical ripple wells. Our experiments and novel theory have now characterized a new kind of neoclassical transport processes arising from *chaotic* (collisionless) separatrix crossings, which occur due to equilibrium $E \times B$ plasma rotation along poloidally asymmetric (*ruffled*) separatrices, and due to wave-induced separatrix modulations.
PACS: 52.25.Fi, 52.27.Aj

1. INTRODUCTION

Neoclassical transport due to axial asymmetries is ubiquitous in magnetic fusion plasma confinement. These plasmas typically have several helically trapped particle (superbanana) populations, either by natural design (stellarators) or due to the finite number of toroidal field coils (tokamaks), partitioned by separatrices from one another and from toroidally trapped (banana) particle trajectories. The drift orbits for particles trapped in the two toroidally separate regions are displaced radially from one another, leading to the conventional neoclassical superbanana ripple transport as particles collisionally change (at rate ν) from helically trapped to toroidally trapped and back. Neoclassical ripple transport theory analyzes the particle transport and wave effects arising from *collisional* scattering across the ripple separatrix in a variety of geometries [1-4], and experimental corroboration has been obtained in some regimes of strong collisions [5, 6].

This situation is dramatically modified when the ripple separatrix is itself poloidally asymmetric (*ruffled*), or when it fluctuates due to waves in the plasma. In such a case the particles see a time-varying separatrix barrier, and without needing collisions they can *chaotically* transit between helically and toroidally trapped populations. This mechanism can substantially modify particle transport in low collisionality regimes associated with fusion plasmas, though it has previously been considered to be ineffective due to a presumed symmetry of such transitions [7].

In our experiments with θ -ruffled separatrix these chaotic crossings lead to considerably enhanced (or noticeably suppressed, for that matter) neoclassical ripple transport, depending on the relative phase α between the toroidal tilt and the separatrix ruffle asymmetries. The experiments utilize externally controlled electrostatic ruffles or fluctuations on the separatrix, and can thus identify the novel chaotic neoclassical ripple transport scaling as $\nu^0 B^{-1} \sin^2 \alpha$, and thus distinct from collisional neoclassical ripple transport scaling as $\nu^{1/2} B^{-1/2}$.

2. EXPERIMENTAL SETUP

The experiments utilize a cylindrical Penning-Malmberg trap to confine quiescent, low-collisionality

pure electron plasmas [8-10]. Electrons are confined radially by a nominally uniform axial magnetic field $0.04 < B < 2$ T; and are confined axially by voltages $V_c = -100$ V on end cylinders of radius $R_w = 0.035$ m. The electron columns have length $L_p = 0.49$ m, and radial density profile $n(r)$ with central density $n_0 \approx 1.6 \times 10^{13} \text{ m}^{-3}$ and line density $N_L = \pi R_p^2 n_0 \approx 6.1 \times 10^9 \text{ m}^{-1}$. The unneutralized charge results in an equilibrium potential energy $\Phi_e(r)$ with $\Phi_{e0} \approx +28$ eV at $r = 0$ (here, all Φ 's are in energy units). This gives an $E \times B$ rotation frequency $f_E(r)$ which decreases monotonically from $f_{E0} \approx 230 \text{ kHz} \times (B/1\text{kG})^{-1}$. The bulk electrons have a near-Maxwellian velocity distribution with thermal energy $T \leq 1$ eV, giving axial bounce frequency $f_b \approx 430$ kHz and rigidity parameter $Rg \equiv f_b / f_E \approx 2B_{\text{kG}}$.

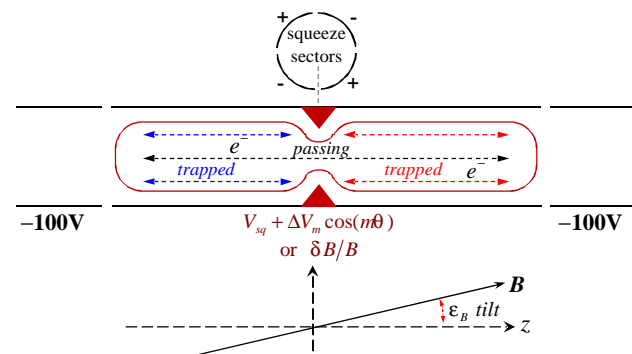


Fig. 1. Schematic of electron plasma with tilt ϵ_B and a trapping barrier in a cylindrical Penning-Malmberg trap

As a helical ripple substitute, an electrostatic trapping barrier $\phi_s(r, \theta)$ is created by a “squeeze” wall voltage V_{sq} (see Fig.1) with adjustable θ -sector voltages $\pm \Delta V_m$. This gives controllable interior separatrix energy $\phi_s(r, \theta) = \phi_{s0}(r) + \Delta \phi_m \cos[m(\theta - \theta_m)]$. Here we focus mostly on $m = 2$ ruffles, created by voltages $\pm \Delta V_2$ applied to four 60° sectors, extending over $\Delta z = 3.8$ cm near the $z = 0$ center. At every radius, low energy particles are trapped in either the left or right end, whereas higher energy passing particles transit the entire length of the column. Ruffles spread the characteristic separatrix energy by $\Delta \phi_m(r) \sim \Delta V_m (r/R_w)^m$, somewhat reduced by plasma shielding.

Particles change from ripple trapped to passing (and vice versa) due to binary collisions at rate ν , due to drift-rotation across θ -ripple variations $\Delta\phi_m$, or due to temporal fluctuations $\Delta\phi(t)$ in the separatrix energy. The electron-electron collisionality in the present experiments is relatively low ($\nu \sim 100/\text{s}$), and collisions acting for a drift-rotation period spread the separatrix by an energy width $\Delta W_c \equiv T(\nu/2\pi f_E)^{1/2}(\phi_{s0}/T)^{1/2} \approx 0.02eV \times (B/1\text{kG})^{1/2}$. Thus, the chaotic (de)trapping processes will be important when $\Delta\phi_m(r) \geq \Delta W_c$, or when $\Delta\phi(t) \geq \Delta W_c$.

We diagnose the bulk expansion rate $\nu_{\langle r^2 \rangle}$ defined as

$$\nu_{\langle r^2 \rangle} \equiv \frac{1}{\langle r^2 \rangle} \frac{d\langle r^2 \rangle}{dt}. \quad (0.1)$$

Fortunately, it can be accurately and readily obtained from the continuous frequency shift $f_2(t)$ of a small amplitude $m=2$ diocotron mode, as $\nu_{\langle r^2 \rangle} = (1/f_2) df_2/dt$. The bulk expansion rate $\nu_{\langle r^2 \rangle}$ is an integral measure of the full radial flux that includes both mobility and diffusive contributions, both being proportional to the radial diffusion coefficient $D_r(r)$.

3. ASYMMETRY-INDUCED TRANSPORT

Radial particle transport is conveniently driven by a global (toroidal) magnetic tilt asymmetry with controlled magnitude $\epsilon_B \equiv B_\perp/B_z \leq 0.001$ and gradually chosen tilt direction $\theta_B \equiv \tan^{-1}(B_y/B_x)$. This tilt is equivalent to applying z -antisymmetric wall voltages $V_a(R_w, \theta, z) = \epsilon_B z (2eN_L/R_w) \cos(\theta - \theta_B)$, which causes interior Debye-shielded z -asymmetric potentials $\delta\phi_a(r, z)$. For large B fields, giving rigidity $Rg \gg 1$, simple z -bounce-averaged theory suffices to describe the separatrix-induced transport and wave-damping. The tilt-induced z -asymmetric error field $\delta\phi_a(r, z)$ has bounce average values $\delta\phi_L$ and $\delta\phi_R$ for left- and right-end trapped particles near the separatrix energy, with passing particles experiencing zero bounce-average error field. The drift orbits then for left- and right-end superbanana trajectories differ radially by

$$\Delta r = (\overline{\delta\phi_L} - \overline{\delta\phi_R}) / \overline{\partial\Phi_e/\partial r}. \quad (0.2)$$

Random transitions between trapped and passing populations are caused by collisions (c); by drift rotation along the $\cos(m\theta)$ separatrix ruffles (m); and by temporal fluctuations in the separatrix energy (t). If the fraction of particles transitioning in a rotation period is η , the radial diffusion coefficient is expected to be

$$D_r \sim \eta f_E \Delta r^2. \quad (0.3)$$

For collisions, conventional neoclassical ripple transport gives $\eta_c = \Delta W_c F_M(\phi_{s0}) \propto \nu^{1/2} B^{1/2}$, where F_M is the Maxwellian distribution of energies, whereas ripple η_m and temporal η_t are independent of ν and B .

A detailed analysis of random transitions between equal trapping regions driven by rotation across separatrix ruffles gives neoclassical asymmetric superbanana radial diffusion coefficient

$$D_r(r) = \frac{1}{4} F_M(\phi_{s0}) f_E \Delta r^2 \times \left\{ \Delta W_c D_{cA} + \Delta\phi_2 D_{2A} \sin^2 \alpha \right\}. \quad (0.4)$$

Both the collisional bounce-Averaged transport coefficient D_{cA} and the $m=2$ ruffle coefficient D_{2A} are shown in Fig. 2, calculated in [11] as functions of the normalized ruffle strength $\Delta\phi_2/\Delta W_c$. While the ruffle-induced transport coefficient D_{2A} is nearly independent of $\Delta\phi_2/\Delta W_c$, the collisional coefficient D_{cA} shows a fast decline as chaotic particle transitions become the dominant ones and smooth out the discontinuity of F_M . In the case of properly aligned asymmetries ($\sin^2 \alpha \approx 0$), this could enable some suppression of collisional neoclassical ripple transport, until bounce-resonant transport processes become significant.

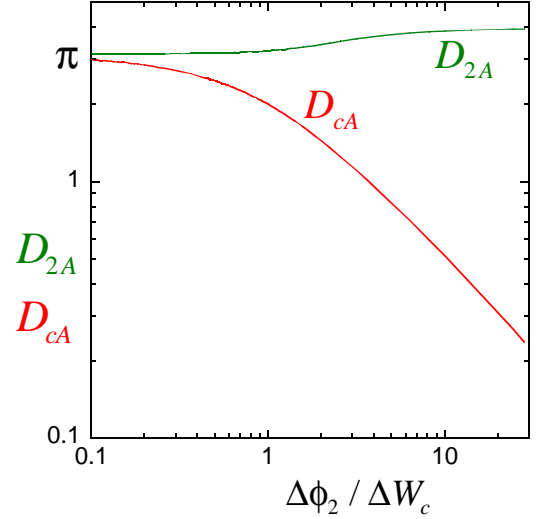


Fig. 2. Calculated collisional D_{cA} and ruffle induced D_{2A} coefficients versus the normalized ruffle strength

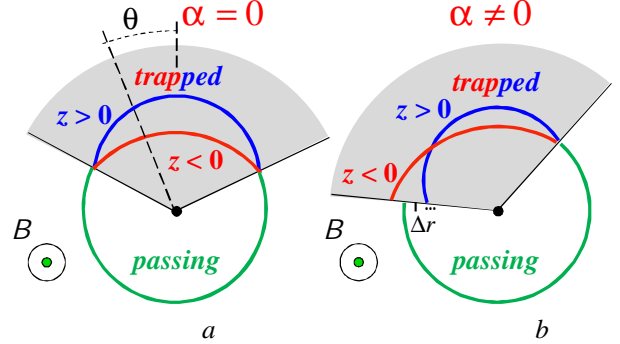


Fig. 3. Sketch of split $E \times B$ drift orbits near the $m=2$ ruffled separatrix. a) $\alpha = 0$. b) $\alpha \neq 0$. For the magnetic tilt asymmetry the trapped portions of the orbits are partial circles shifted along the tilt direction

Prior theory [7] considered only $\alpha = 0$ or π , in which case the phase-dependent part of the diffusion coefficient is zero. The reason for this can be qualitatively understood from Fig. 3,a, which shows a sketch of split $E \times B$ drift orbits near the $m=2$ ruffled separatrix. From the magnetic tilt asymmetry the trapped portions of the drift orbits are partial circles shifted along the tilt direction. If this direction coincides with the zero phase of separatrix ruffle, the left-right symmetry implies particles transit from trapped to passing and back at the same radius, so the drift orbit is closed and there is no net radial step. However, when $\alpha \neq 0$, the symmetry is broken and particle orbits are trapped and detrapped at different radii, leading to radial steps $\Delta r \neq 0$ (Fig. 3,b). Of course, for

$\alpha=0$ or π the diffusion does not completely vanish; collisional effects not kept in the above analysis yield finite diffusion consistent with the one obtained in [7].

Fig. 4 shows the predicted transition from predominantly collisional neoclassical diffusion to the chaotic regime (ruffle dominated, $D_r \propto \Delta\phi_2 D_{2A}$). For comparisons with the experiments it can be rather conveniently approximated as

$$D_* \equiv \Delta W_c D_{cA} + \Delta\phi_2 D_{2A} \sin^2 \alpha \quad (0.5)$$

$$\approx 4(\Delta\phi_2 \sin^2 \alpha + 0.88\Delta W_c e^{\frac{\Delta\phi_2}{0.88\Delta W_c}}).$$

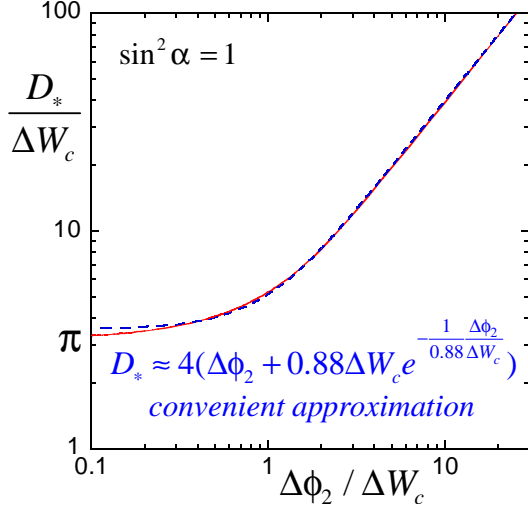


Fig. 4. Combined neoclassical ripple transport coefficient D_* versus the normalized ruffle strength. The dashed line shows derived approximation

Fig. 5 shows the measured expansion rate $v_{\langle r^2 \rangle}$ for the case $\sin^2 \alpha = 1$ as a function of ruffle voltages $\pm \Delta V_2$ at the wall. It has essentially the same fitting function as in Fig. 4, giving the normalized “radially averaged” ruffle strength as $\langle \Delta\phi_2 / \Delta W_c \rangle_r \approx (4/3)\Delta V_2 / 1V$, which is close to its calculated value. Thus, at $B = 6$ kG and $\Delta V_2 = 3V$ the effective ruffle width $\Delta\phi_2 \approx 4\Delta W_c$, and the transport rate has changed by $4\times$ accordingly.

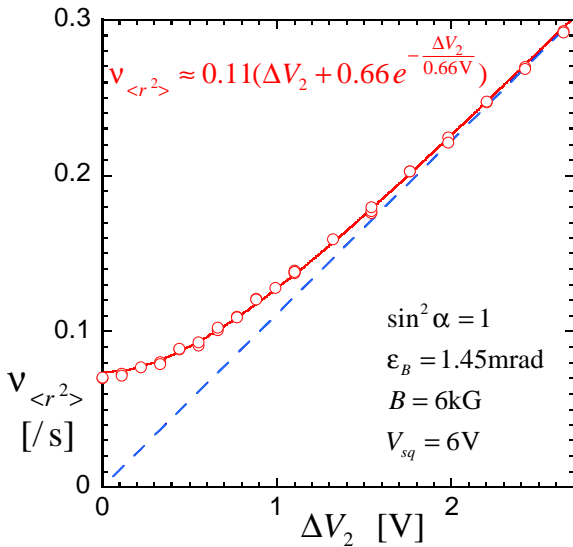


Fig. 5. Measured expansion rate as a function of the ruffle voltage ΔV_2 at the wall

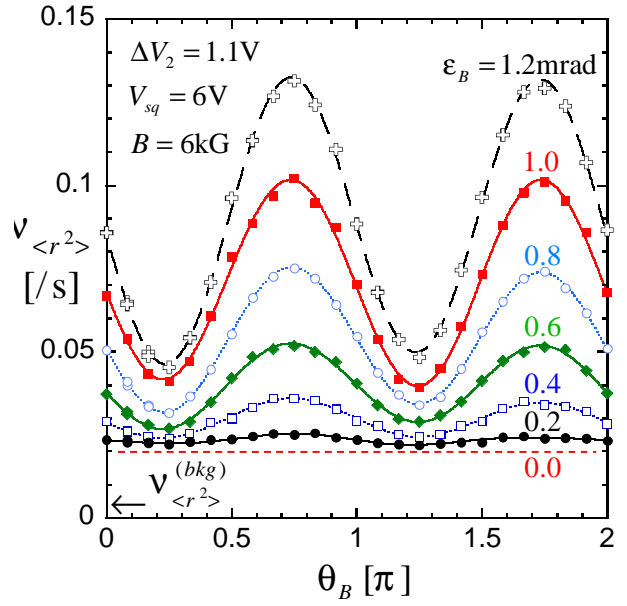


Fig. 6. Measured expansion rate $v_{\langle r^2 \rangle}$ at fixed $\Delta V_2 = 1.1V$ showing chaotic part of neoclassical transport varying as $\epsilon_B^2 \sin^2 \alpha$, and α -independent collisional ripple transport

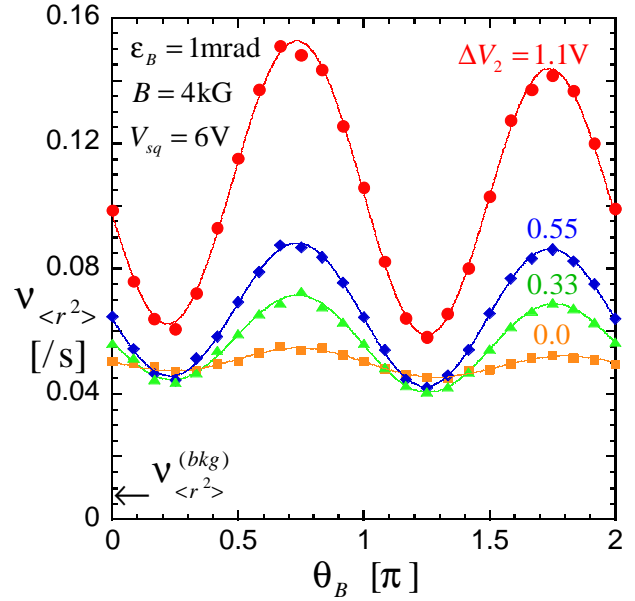


Fig. 7. Measured expansion rate $v_{\langle r^2 \rangle}$ at fixed $\epsilon_B = 0.001$, showing chaotic part of neoclassical transport varying as $\Delta V_2 \sin^2 \alpha$, and α -independent collisional ripple transport

Fig. 6 is a plot of measured expansion rate $v_{\langle r^2 \rangle}$, taken during step-by-step rotation of the magnetic tilt orientation angle θ_B , for various tilt strengths ϵ_B at the fixed wall ruffle $\Delta V_2 = 1.1V$. The ruffled-induced part shows an unambiguous $\sin^2 \alpha$ dependence on relative angle $\alpha \equiv \theta_B - \theta_2$, (here, $\theta_2 \approx \pi/4$) with magnitude proportional to ϵ_B^2 ; and varying θ_2 in steps of $\pi/2$ (not shown) verifies the dependence on relative angle only.

Fig. 7 is a plot of measured expansion rate $v_{\langle r^2 \rangle}$ versus magnetic tilt orientation angle θ_B , for various applied wall ruffle strengths ΔV_2 , now at the fixed tilt strength $\epsilon_B = 0.001$. Once again, the ruffled-induced part shows unambiguous $\sin^2 \alpha$ signature, but now with magnitude proportional to ΔV_2 .

The distinctive $\varepsilon_B^2 \sin^2 \alpha$ signature, together with separate control of ΔV_2 and ε_B , enables experimental identification of neoclassical transport processes separately from z-kinetic processes. We model the full transport as

$$v_{\langle r^2 \rangle} = C_{cA} (\Delta V_2) \varepsilon_B^2 + C_{2A} \varepsilon_B^2 \Delta V_2 \sin^2 \alpha + C_{cK1} \varepsilon_B^2 + C_{cK2} \Delta V_2^2 + v_{\langle r^2 \rangle}^{(bkg)}, \quad (0.6)$$

where C_{cA} and C_{2A} represent the radial integrals of Eqn. (1.4); C_{cK1} and C_{cK2} represent collisional Kinetic (bounce-resonant) transport driven by ε_B^2 and ΔV_2^2 as z-dependent ‘‘error’’ fields [12-14]; and small $v_{\langle r^2 \rangle}^{(bkg)}$ arises from uncontrolled background tilts, separatrices, and omnipresent ruffles. Here, for dimensional simplicity, $\varepsilon_B \equiv \varepsilon_B / (1\text{mRad})$ and $\Delta V_2 \equiv \Delta V_2 / (1\text{Volt})$.

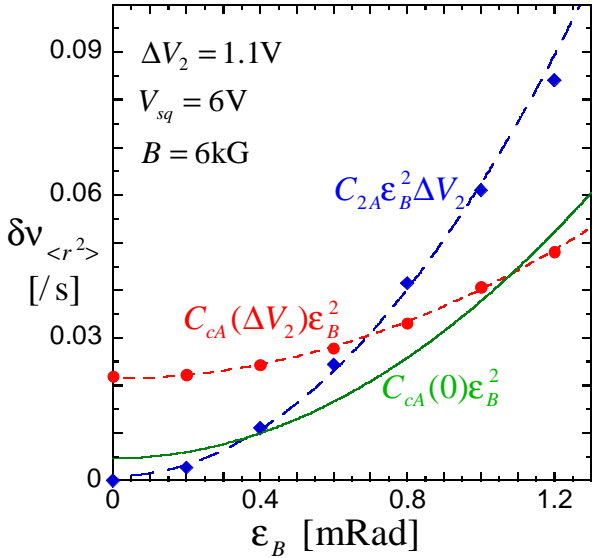


Fig. 8. Measured ε_B^2 scalings for the C_{2A} and $C_{cA}(\Delta V_2)$ neoclassical helical ripple transport terms at $B = 6\text{ kG}$. Every marker here (not shown for $C_{cA}(0)$) is the result of $(a + b \sin^2 \alpha)$ fit as those shown in Fig. 6

C_{2A} and $C_{cA}(\Delta V_2)$ are readily obtained from the $\sin^2 \alpha$ dependences as those shown in Figs. 6 and 7, and varying ε_B gives the expected ε_B^2 scaling, as the one shown in Fig. 8 for $\Delta V_2 = 1.1\text{ V}$ and $B = 6\text{ kG}$ ($C_{2A} \approx 0.056/\text{s}$). Data taken with $\Delta V_2 = 0$ define $C_{cA}(0) \approx 0.033/\text{s}$; and just by comparing it to $C_{cA}(1.1\text{V}) \approx 0.019/\text{s}$ and using the $D_{cA}(\Delta \phi_2 / \Delta W_c)$ data from Fig. 2, one can get another estimate on the ‘‘radially averaged’’ ruffle strength as $\langle \Delta \phi_2 / \Delta W_c \rangle_r \approx (4/3) \Delta V_2 / 1\text{V}$, which is consistent with the previous conclusion based on the results in Figs. 4 and 5.

Data taken with $\varepsilon_B = 0$ show a $v_{\langle r^2 \rangle}^{(bkg)}$ offset and a parabolic dependence on a varied ΔV_2 , giving C_{cK2} . Varying ε_B then selects C_{cA} and C_{cK1} ; these terms are distinguished by their B -scaling (discussed next), and by the fact that the z-antisymmetric bounce-averages in C_{cA} require the separatrix, whereas the kinetic C_{cK1} depends only weakly on the applied squeeze voltage. In Fig. 7, $C_{cK2}(4\text{kG}) \approx 0.03$, giving elevated $\sin^2 \alpha$ minima for large ΔV_2 ; the depressed minima for $\Delta V_2 = 0.33$ are from ruffle-suppression of D_{cA} (see Fig. 2); and $v_{\langle r^2 \rangle}^{(bkg)} \approx 0.007/\text{s}$.

Fig. 9 shows the measured transport rates C_{2A} , C_{cA} and C_{cK1} versus magnetic field with empirical scalings

(dashed), compared to theory (solid lines). At high B , the chaotic and collisional separatrix transport processes agree closely with theory, scaling as B^{-1} and $B^{-1/2}$ respectively. Here the accuracy of comparison is limited by temperature uncertainty, sensitivity to edge density gradients, and induced modification of $F_M(\phi_{s0})$. At low B , the kinetic transport labeled C_{cK1} is observed to depend strongly on field ($\propto B^{-2.7}$), but no simple power law is expected theoretically as bounce-rotation resonances become dominant. Prior scaling experiments have been confused by the presence of uncontrolled separatrices and ruffles, as well as by overlapping transport regimes [8].

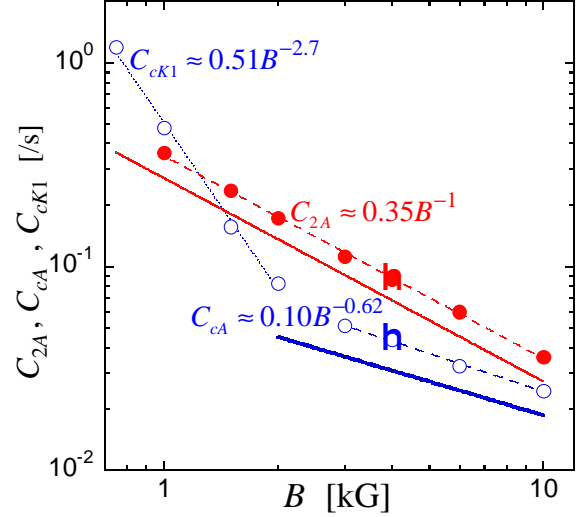


Fig. 9. Measured transport rates C_i versus B at $V_{sq} = 6\text{ V}$, with empirical scalings. Solid lines are theory predictions

Similar enhanced particle transport is observed when there are temporal variations in the separatrix energy. Fig. 10 illustrates the immediate increase in radial expansion rate induced when white noise ($V_{\text{RMS}} = 0.2\text{ V}$, $f_E < f < 20\text{ MHz}$) is applied to the θ -symmetric ripple (squeeze) ring, driving randomly enhanced collisionless separatrix crossings.

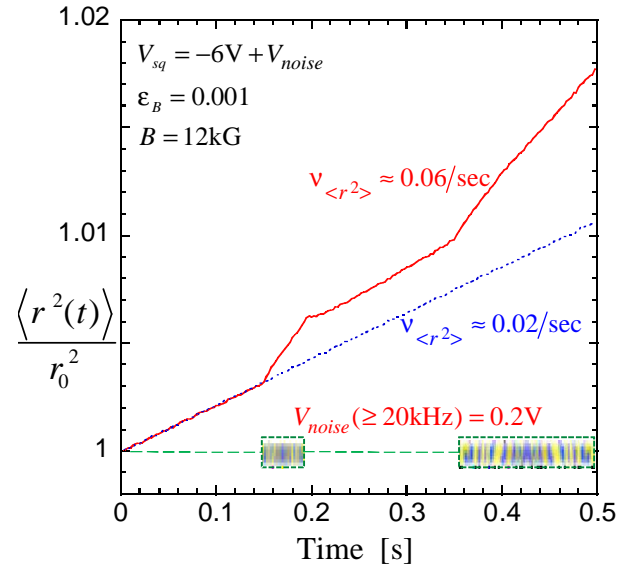


Fig. 10. Enhanced expansion rate during two bursts of 0.2 V (RMS) white noise $\Delta \phi(t)$ applied to a $V_{sq} = 6\text{ V}$ electrostatic ripple

The $3\times$ increase in $(d/dt)\langle r^2 \rangle$ rate observed here is consistent with a collisional separatrix layer width $\Delta W_c \approx 0.07$ eV fluctuating by $\Delta\phi(t) \approx 0.2$ eV. Presumably, any noise- or wave-induced fluctuations which change particle kinetic energies relative to the separatrix energy would be equally effective in enhancing neoclassical helical ripple transport.

4. CONCLUSIONS

Most plasma confinement devices have trapping separatrices (ripples), arising from variations in magnetic field strength or external potentials. These separatrices are never perfectly symmetric, or perfectly aligned with other asymmetries. If the separatrix itself is asymmetric or temporally perturbed, the drifting particles collisionlessly change from trapped to passing and back, leading in the case of low collisionality ($v/f_E \ll 1$) to enhanced asymmetric superbanana ripple transport ($\propto v^0 B^{-1}$) in comparison to the standard neoclassical ripple transport ($\propto v^{1/2} B^{-1/2}$). When the separatrix layer collisional width is less than its θ -asymmetry or temporal perturbations, this new loss mechanism becomes the dominant bulk transport process in our non-neutral plasma experiments, and it could have important implications for similar low collisionality regimes in other magnetic confinement experiments.

ACKNOWLEDGMENTS

This work was supported by National Science Foundation Grant PHY-0903877 and Department of Energy Grant DE-SC0002451.

REFERENCES

1. P. Helander, D.J. Sigmar. *Collisional Transport in Magnetized Plasmas*, Cambridge: "Cambridge University Press", 2002.
2. M.N. Rosenbluth, D.W. Ross, D.P. Kostomarov. Stability regions of dissipative trapped-ion instability// *Nuclear Fusion*, 1972, v. 12, N1, p. 3-37
3. T.J. Hilsabeck, T.M.O'Neil. Trapped-particle diocotron modes// *Physics of Plasmas*. 2003, v. 10, N9, p. 3492-3505.
4. D.H.E. Dubin. Theory and simulations of electrostatic field error transport// *Physics of Plasmas*. 2008, v. 15, N7, p. 072112-26.
5. T. Ohkawa, J.R. Gilleland, T. Tamano. Observation of neoclassical, intermediate, and Pfirsch-Schulter diffusion in the dc octopole// *Physical Review Letters*. 1972, v. 28, N17, p.1107-1111.
6. M.C. Zarnstorff, K. McGuire, et. al. Parallel electric resistivity in the TFTR tokamak// *Physics of Fluids B*. 1990, v. 2, N8, p. 1852-1857.
7. H.E. Mynick. Effect of collisionless detrapping on non-axisymmetric transport in a stellarator with radial electric field// *Physics of Fluids*. 1983, v. 26, N9, p. 2609-2615.
8. A.A. Kabantsev, C.F. Driscoll. Trapped-particle modes and asymmetry-induced transport in single-species plasmas// *Physical Review Letters*. 2002, v. 89, N24, p. 245001-4.
9. A.A. Kabantsev, T.M. O'Neil, Yu.A. Tsidulko, C.F. Driscoll. Resonant drift-wave coupling modified by non-linear separatrix dissipation// *Physical Review Letters*. 2008, v. 101, N6, p. 065002-4.
10. A.A. Kabantsev, C.F. Driscoll. Trapped-particle mediated collisional damping of nonaxisymmetric plasma waves// *Physical Review Letters*. 2006, v. 97, N9, p. 095001-4.
11. D.H.E. Dubin, C.F. Driscoll, Yu.A. Tsidulko. Neoclassical transport caused by collisionless scattering across an asymmetric separatrix// *Physical Review Letters*. 2010, v. 105, N18, p. 185003-4.
12. D.L. Eggleston, T.M. O'Neil. Theory of asymmetry-induced transport in a non-neutral plasma// *Physics of Plasmas*. 1999, V. 6, N7, p. 2699-2704.
13. D.L. Eggleston, J.M. Williams. Magnetic field dependence of asymmetry-induced transport: a new approach// *Physics of Plasmas*. 2008, v. 15, N3, p. 32305-6.
14. E.P. Gilson, J. Fajans. Quadrupole-induced resonant-particle transport in pure electron plasma// *Physical Review Letters*. 2003, v. 90, N1, p. 015001-4.

Article received 13.09.10

ЭКСПЕРИМЕНТЫ ПО НЕОКЛАССИЧЕСКИМ ПЕРЕНОСАМ НА ВОЗМУЩЕННЫХ СУПЕРБАНАНОВЫХ ТРАЕКТОРИЯХ В ЭЛЕКТРОННОЙ ПЛАЗМЕ

А.А. Кабанцев, Ч.Ф. Дрисколл

Гофрировка тороидального поля приводит к появлению локально-запертых частиц, и традиционная неоклассическая диффузия описывает процессы переноса, обусловленные их кулоновскими столкновениями на супербанановых орбитах. В наших экспериментах с аксиально-несимметричной гофрировкой исследованы новые эффекты хаотического (бесстолкновительного) неоклассического переноса, вызванные как ЕХВ вращением электронной плазмы вдоль полоидально-возмущенных сепаратрисс, так и на сепаратриссах, возмущаемых волновыми взаимодействиями (микрофлуктуациями) в плазме.

ЭКСПЕРИМЕНТИ З НЕОКЛАСИЧНИМИ ПЕРЕНОСАМИ НА ОБУРЕНИХ СУПЕРБАНАНОВИХ ТРАЕКТОРИЯХ В ЕЛЕКТРОННІЙ ПЛАЗМІ

А.А. Кабанцев, Ч.Ф. Дрисколл

Гофрування тороидального поля приводить до появи локально-замкнених часток, і традиційна неокласична дифузія описує процеси переносу, обумовлені їх кулоновськими зіткненнями на супербананових орбітах. У наших експериментах з аксиально-несиметричним гофруванням досліджені нові ефекти хаотичного (беззіттовхувального) неокласичного переносу, викликані як ЕХВ обертанням електронної плазми уздовж полоїдально-збурених сепаратрис, так і на сепаратриссах, що збурені хвильовими взаємодіями (мікрофлуктуаціями) у плазмі.